ISSN: 2754-4753

Journal of Physics & Optics Sciences

Research Article

Open Access

Analysis of Muon Detection at Ground Level from Proton and Iron Showers for Primary Energies between 100 GeV and 100 TeV

Hector Apaza Ortiz[1]*, Rolando Perca Gonzales[1], Ronald Pastor Rodriguez[1], Jose Bellido Caceres[2] and Luis Otiniano Ormachea[3]

[1]National University of San Agustín de Arequipa, Santa Catalina 117, Arequipa 04000, Arequipa, Peru

[2]Neo Analytics, North Terrace, Adelaide SA 5000, Adelaide, Australia

[3]CONIDA, Calle Luis Felipe Villaran 1069, San Isidro 15046, Lima, Peru

ABSTRACT

Understanding the proportion of muons within atmospheric showers is crucial for determining the primary composition of cosmic rays and for discriminating between gamma and hadronic events. While iron-induced showers typically produce more muons than proton-induced ones, we found that below approximately 1 TeV, proton showers exhibit a higher number of muons arriving at the detector. This discrepancy arises from the lower energy of muons generated by low-energy iron showers, leading to many of these muons decaying before reaching the detector level. Consequently, the sensitivity to iron showers in water Cherenkov detectors is significantly reduced below approximately 1 TeV, a factor that must be considered when estimating the cosmic ray energy spectrum in this lower energy range. This study uses CORSIKA simulations to quantify the size of the muonic component at the detector level for both proton and iron showers, taking into account the shower energy and various detector altitudes.

***Corresponding author**

Hector Apaza Ortiz, National University of San Agustín´ın de Arequipa, Santa Catalina 117, Arequipa 04000, Arequipa, Peru.

Received: March 10, 2025; **Accepted:** March 14, 2025; **Published:** August 10, 2025

Keywords: Cosmic Rays, Simulations, CORSIKA, Extensive Air Shower, Muonic Component

Introduction

Cosmic rays (CRs) are primarily relativistic atomic nuclei originating from outer space. These particles strike Earth almost isotropically and account for about 1% of the total mass of the universe [1]. Most of these particles are ionized nuclei: around 90% are protons, 9% are alpha particles, and the rest are heavy nuclei, which are characterized by carrying high energies [2]. The energies of cosmic rays can range from a few MeV to several ZeV. Two main methods are used to detect them. For energies above 100 TeV, the indirect method is dominant, based on the measurement of atmospheric showers [3]. On the other hand, the direct method, applicable to energies below 1000 TeV, uses particle detectors aboard balloons, spacecraft, and satellites [4,5].

When cosmic rays penetrate Earth's atmosphere, they trigger a cascade of particles known as an extensive air shower (EAS). These showers consist of a variety of particles, with the electromagnetic component and the muonic component being the primary carriers of energy of the showers to the ground. The proportion of muons in these cascades is crucial for differentiating between electromagnetic showers and hadronic showers, even for distinguishing between showers initiated by heavy versus light hadrons. In this context, the superposition model treats a high-energy nucleus (such as an iron nucleus) as if it were a collection of individual nucleons (protons and neutrons), which interact independently with the atmosphere, so that an EAS initiated by a heavy nucleus like iron is a superposition of 56 proton showers. In hadron-initiated cascades, a significant fraction of the energy reaches the surface in the form of muons. However, according to [6], the contribution from heavier elements significantly decreases below 1 TeV, so very few particles reach the Earth's surface. According to The High-Altitude Water Cherenkov Gamma-Ray Observatory (HAWC) results [7], above 1 TeV, the detection efficiency between light and heavy primaries is higher for protons than for iron nuclei, and this difference decreases as the primary energy increases. The reasons for these characteristics will be addressed in this research.

The primary objective of this research is to quantify and parameterize the reduction in the muonic component of air showers initiated by heavy nuclei, such as iron, compared to lighter particles like protons, particularly for energies below 1 TeV, an energy region in which, according to [8], the difference between proton and iron nucleus cascades becomes more pronounced. This analysis is conducted as a function of detector altitude, leveraging the advantages of high-altitude observatories. Understanding the variation of the muonic component is crucial for determining the composition of low-energy cosmic rays and for improving the reconstruction of individual particle energy spectra. Recent observations, such as those from the Large High Altitude Air Shower Observatory (LHAASO) and HAWC experiments, have shown that heavy nuclei produce a higher muon-toelectron ratio in extensive air showers, which can be effectively used to distinguish between different primary cosmic ray compositions [9]. These findings are pivotal in advancing our understanding of the origins and propagation of cosmic rays, especially at low energies, where the composition and spectrum are still subjects of active research.

This study utilizes the COsmic Ray SImulations for KAscade (CORSIKA) program to simulate EAS initiated by primary cosmic rays, including iron, nitrogen, helium, and protons, with energies spanning from 100 GeV to 100 TeV. This energy range is well-suited to the operational capabilities of high-altitude observatories like LHAASO and Southern Wide-field Gamma-ray Observatory (SWGO), which cover a similar spectrum from tens of GeV up to the PeV scale [10,11]. The simulations were conducted at observation levels corresponding to altitudes of 0, 4800, 6000, and 10000 meters above sea level (masl), allowing for a detailed examination of the evolution of EAS as a function of altitude.

Extensive Air Shower Simulations

This research uses version 77420 of CORSIKA, updated on May 20, 2022. For low-energy interactions, the Ultrerelativistic-Quantum Molecular-Dynamics model (UrQMD) [12] was used, while for high energies, the Quark Gluon String model with JETs - II model (QGSJET-II) [13] was employed. In CORSIKA, the energy transition between high and low energy is around 80 GeV [14]. These models were chosen due to their acceptance in the expert community, availability in CORSIKA, and computational efficiency.

To study the decrease in muons at different altitudes in showers initiated by heavy primaries compared to light primaries, simulations were conducted at altitudes of 0, 4800, 6500, and 10000 masl. The altitude of 4800 masl corresponds to a region in the district of Yanque in Arequipa, Peru (15° 43'46.8"S 71°37'24.0W), a candidate for hosting future SWGO facilities. The simulations focused on specific energies from 100 GeV to 100 TeV, with discrete intervals of 0.025 on the logarithmic scale (log10), performing 1000 simulations per energy for each particle. The simulated primaries were iron, nitrogen, helium, and protons, focusing on comparisons between protons and iron nuclei.

The thinning method was used, with a thinning factor $\varepsilon_{th} = 10^{-2}$ (detailed information on this method can be found in [15,16]. The cut-off energies were 300 MeV for hadrons and muons, and 3 MeV for electrons and gamma rays. The Earth's magnetic field values were obtained using the National Oceanic and Atmospheric Administration (NOAA) web tool for the established geographic coordinates of Yanque [17]. This tool provided magnetic field values of ~ 22.955 nT for the north component and ~ −3.849 nT for the vertical component.

Muon Component Simulation

Muons are primarily produced in hadronic cascades, resulting from the decay of charged pions and kaons. A primary hadron travels through the atmosphere and, upon interaction, generates charged pions, which either interact or decay, producing muons. This process repeats until the energies of the pions fall below a critical energy, ξ_c^π, which mainly depends on atmospheric density and the intrinsic properties of the pions. Below this energy, they decay solely into muons. This energy marks the stage of the shower where most muons are generated [18]. In addition to charged pions, neutral pions are also produced, which immediately decay into photons, forming electromagnetic cascades.

The muon distribution at the production point transforms into the distribution at the detection point through various interactions during propagation in the atmosphere, such as energy loss, decay, scattering, geomagnetic deflection, and Bremsstrahlung. Muons that survive all interactions reach the detection level with some energy E, which must be below a threshold energy Eth ≈ 160 MeV to generate a signal detectable by Cherenkov detectors. In CORSIKA, inelastic hadronic interactions of muons are omitted due to their rarity. Only Bremsstrahlung interactions, pair production (e−, e+), and muon decay $\mu^\pm \rightarrow e^\pm + \nu e + \nu\mu$ [16] are considered. Due to the kinematics of the original mesons, most muons are generated a few meters from the shower axis [19]. Additionally, they exhibit universal characteristics, such as the spatial distribution of muons at the detection level not depending on the type of primary or its energy [18].

Proton and iron showers develop longitudinally in a similar manner until reaching an atmospheric depth XMAX ~ 500 g/cm^2. Beyond this point, proton showers at different primary energies maintain a similar shape among themselves but differ significantly from iron showers [18]. The superposition model [20] posits that an atomic nucleus with A nucleons should behave as A individual nucleons traveling in parallel, and therefore, these nuclei should produce more muons than a nucleus with fewer nucleons. However, iron showers are not simply a combination of lower-energy proton showers. The iron nucleus is expected to gradually disintegrate into smaller nuclei during successive interactions. As a result, a significant part of the hadronic cascade starts lower in the atmosphere [21].

Results

We simulated showers initiated by iron and proton nuclei, covering an energy range from 100 GeV to 100 TeV with discrete energy steps of 0.025 on the logarithmic scale ($\log_{10}$), and at altitudes of 0, 4800, 6000, and 10000 masl. The goal is to understand why, below a certain critical primary energy Eα, as shown in Figure 1, the muonic contribution from heavier nuclei decreases compared to lighter nuclei. The following graph illustrates this behavior.

In Figure 1a (0 masl), it is observed that when the primary energy falls below approximately 2.11 TeV (critical energy Eα), proton-induced showers exhibit a higher muon count compared to showers initiated by heavier nuclei. At 4800 masl. (Figure 1b), this critical energy decreases to 1 TeV. At 6500 masl. (Figure 1c), the critical energy is reduced to 0.75 TeV. Finally, at 10000 masl. (Figure 1d), the critical energy decreases further to less than 0.45 TeV, as shown in Figure 2. Although heavier nuclei like iron have more nucleons and can produce more secondary particles in the initial interactions, this massive initial production does not always result in more muons at the ground level.

In the range of hundreds of GeV, the difference in muon deposition at the ground is more pronounced when comparing proton-induced showers with those induced by iron. At significantly low primary energies, iron deposits nearly 1000 times fewer muons than protons at all detection levels. Figure 1 shows that this behavior is also observed with other nuclei such as nitrogen and helium. At 0 masl, the critical energies (E_α) are 0.79 TeV for proton-nitrogen and 0.33 TeV for proton-helium. At 4800 masl, these critical energies are reduced to 0.4 TeV and 0.2 TeV, respectively. At 6500 masl, they decrease to 0.28 TeV and 0.14 TeV, and at 10000 masl, they are further reduced to 0.17 TeV and 0.1 TeV. Furthermore, the difference in muon deposition is not only notable when comparing protons with heavier nuclei, but also when comparing the muon deposition from a light hadron like helium with that from heavier nuclei such as nitrogen or iron.

Figure 2 shows how the primary energy (E_α) at which heavier nuclei begin to deposit more muons than protons decrease with altitude. This phenomenon occurs because showers initiated by lowerenergy nuclei generate low-energy muons (below 2 GeV, Figure 3), which have a higher probability of decaying before reaching the ground. The relativistic factor γ for a 2 GeV muon is 19, extending its lifetime from 2.2 μs to 41.8 μs, allowing it to travel approximately 8000 m before decaying; for 1 GeV muons, this distance is reduced to 4000 m. Figure 4 indicates that only iron-induced showers with energies above 5 TeV produce muons with average energies greater than 4 GeV, especially at

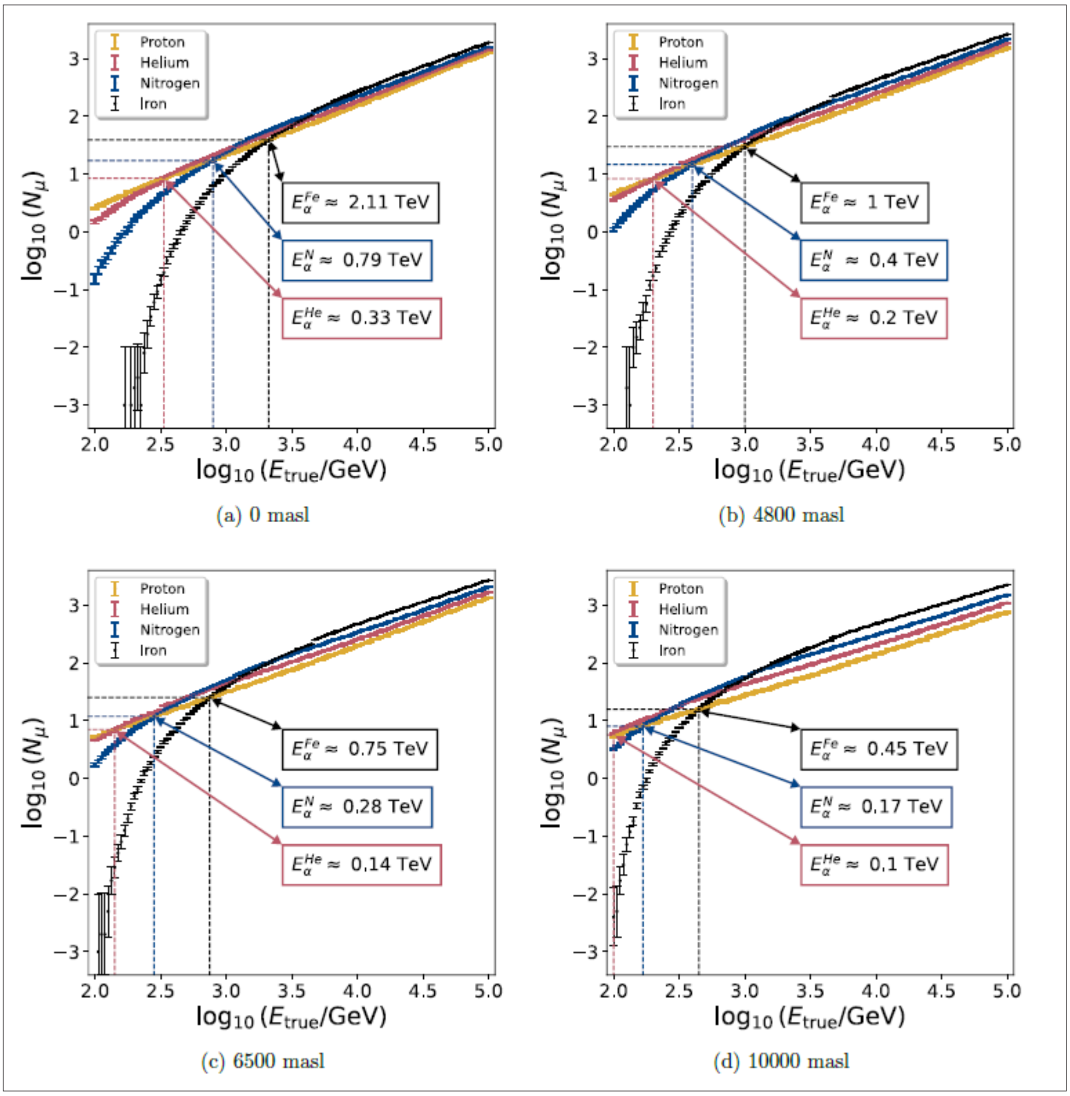

Figure 1: Comparison of the number of muons N_μ deposited at the detection level as a function of the primary energy E_{true} for particles of different masses and at different altitudes.

10000 masl, allowing a significant portion of these muons to reach the ground. To complement this relationship, a second-degree polynomial regression was performed on the three curves.

$$E_\alpha = A * Height2 + B * Height + C \qquad (1)$$

where the fitting constants for all the curves in Figure 2 are shown in Table 1.

Figure 3 shows the energy distribution of muons deposited at 0, 4800, and 10000 masl. To compare the muon counts in showers induced by protons and iron nuclei at energies close to $E_{true} \sim 1$ TeV, showers with a primary energy of 0.5 TeV were selected. It is important to note that, as shown in Figure 1, proton showers generate more muons than those induced by iron nuclei at different detection altitudes for energies close to 1 TeV.

Overall, at an altitude of 10000 masl, showers initiated by iron nuclei contain a significantly higher number of muons (Figure 3). However, these muons exhibit lower energies (below 2 GeV) compared

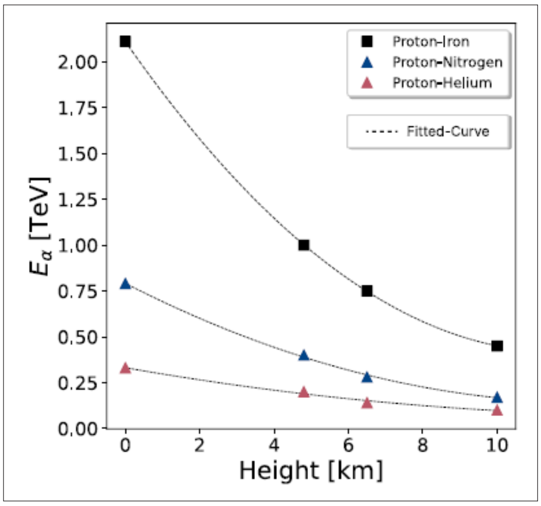

Figure 2: Critical Primary Energy E_α as a Function of Simulation Altitude

Table 1: Fitting Constants for the Curves in Figure 2

Particles	$A \times 10^{-2}$ TeV/km²	$B \times 10^{-1}$ TeV/km	C TeV	R^2
Proton-Iron	1.246 ± 0.014	−2.906 ± 0.014	2.110 ± 0.003	0.999
Proton-Nitrogen	0.412 ± 0.069	−1.036 ± 0.071	0.791 ± 0.016	0.998
Proton-Helium	0.120 ± 0.069	0.354 ± 0.071	0.331 ± 0.016	0.991

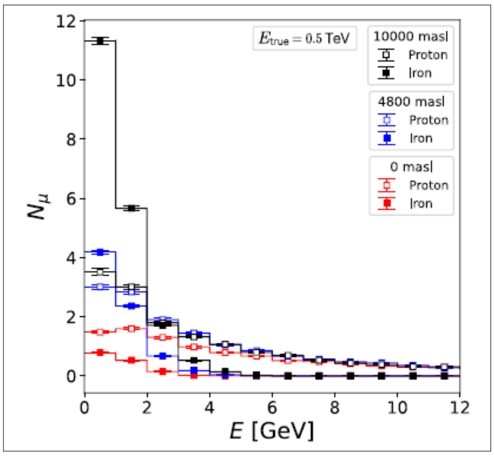

Figure 3: Muon Energy Distribution for Protons and Iron Nuclei at Different Altitudes

to those found in showers initiated by protons at the same altitude. Consequently, as the showers progress through the atmosphere, the disparity in muon counts decreases. Notably, at 0 masl, the number of muons in showers induced by iron nuclei decreases to the point where even the muon count from proton-induced showers surpasses it.

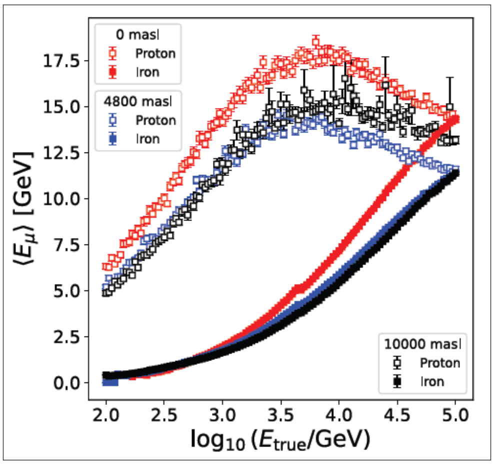

Figure 4: Comparison of the average energy of muons deposited by iron nuclei and protons at different altitudes.

Figure 4 compares the average energy of muons $\langle E_\mu \rangle$ as a function of the primary energy E_{true} for showers induced by protons and iron nuclei at three observation levels: 0, 4800, and 10000 masl. This figure shows that at all observation levels, muons in showers induced by protons have, on average, higher energies than muons in showers initiated by iron nuclei. This observation, along with what is shown in Figure 3, is consistent with the superposition model, where showers initiated by iron nuclei tend to produce a larger number of muons, which are low-energy compared to those in showers initiated by protons, thereby reducing the average energy. Additionally, Figure 4 highlights that at 0 masl, the average energy of muons in showers initiated by iron nuclei is higher than at 4800 and 10000 masl. This is because lower-energy muons, especially at higher altitudes, decay rapidly as they traverse the atmosphere, raising the average energy at lower altitudes.

Figure 5 shows the average energy of muons as a function of primary energy for different primary particles at an altitude of 4800 masl (altitude of Yanque). This figure illustrates that the average energy of muons increases with primary energy but decreases after a certain range due to the production of low-energy muons. Additionally, the average energy of muons is higher when the primary particle is less massive, although heavier particles produce more low-energy muons. Comparing cascades initiated by protons and iron nuclei, the average energy of muons is similar around 100 TeV. At 50 TeV and 27.5 TeV, muons are on average more energetic in nitrogen and helium cascades, respectively. Above these energies, heavier nuclei produce more energetic muons than protons. This behaviour is explained with the help of Figures 6.

The Figure 6 shows the longitudinal distribution of showers initiated by iron nuclei and protons up to 0 masl for primary energies of 0.5 TeV and 10 TeV, which are below and above the 1 TeV threshold, respectively. Atmospheric showers continue to lose energy after reaching their maximum depth, decaying as they penetrate the atmosphere. Figure 6a shows that showers initiated by iron nuclei and protons at 0.5 TeV reach their maximum number of muons at a depth (XMAX) of ~ 180 g/cm² and ~ 370 g/cm², which is equivalent to an altitude of ~ 13.01 km and ~ 8.33 km above sea level, respectively. Figure 6b corresponds to iron and protons at 10 TeV, where the maximum number of muons is recorded at ~ 340 g/cm² and ~ 560 g/cm², which is equivalent to ~ 8.94 km and ~ 5.16 km above sea level. It is observed that showers initiated by iron nuclei reach their maximum number of muons faster than showers from protons at the same energy. This is because when the iron nucleus enters the atmosphere, it fragments rapidly into low-energy nucleons compared to the energy carried

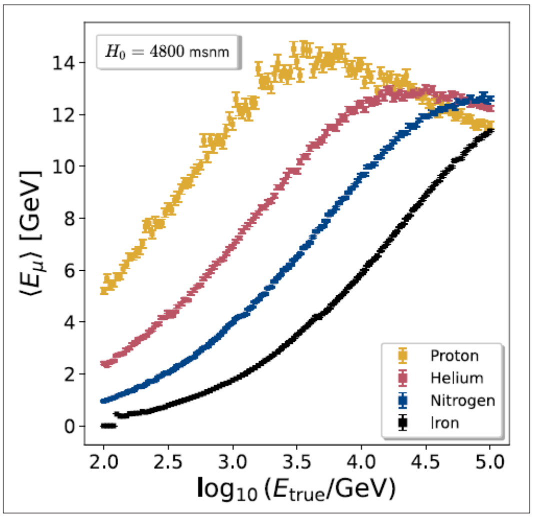

Figure 5: Average Muon Energy $\langle E_\mu \rangle$ as a function of the Primary Energy E_{true}.

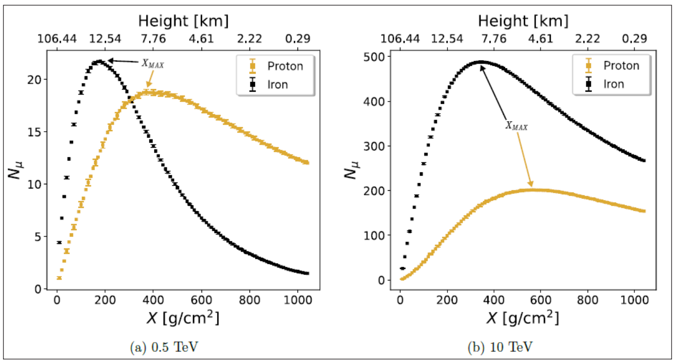

Figure 6: Longitudinal Distribution of showers initiated by Protons and Iron Nuclei at 0.5 TeV (a) and 10 TeV (b) at an altitude of 0 masl, with a selected step length of 10 g/cm^2.

by the proton with the same primary energy. This causes the nucleons from iron to produce more muons, which decay faster than those produced by protons due to their lower energy. This effect is more notable at an energy of 0.5 TeV ($E_{\text{true}} \sim E\alpha$), where the number of iron muons decreases rapidly, resulting in fewer muons detected at all studied observation levels. However, at energies of 10 TeV ($E_{\text{true}} \sim E\alpha$), the muons produced by iron nuclei are energetic enough to reach the observation levels in greater numbers than those produced by protons. Both figures are consistent with the observation in Figure 3, which shows that the number of muons varies significantly with altitude. This is due to the fact that low-energy muons produced by iron nuclei decay rapidly as they traverse the atmosphere. Figure 7 shows the energy lost by muons in a 3-meter-high Cherenkov Water Detector (WCD) as

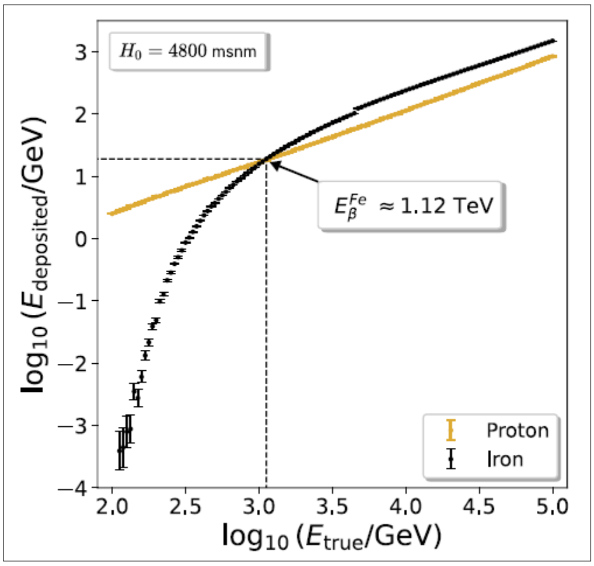

Figure 7: Energy lost by muons in a WCD as a function of primary energy

a function of primary energy, at an observation level of 4800 masl. This energy loss acts as a proxy for the signal generated in the WCD. At energies below approximately 1 TeV, iron nuclei produce fewer muons than protons, as shown in Figure 1b. Only muons with more than 160 MeV generate signals in Cherenkov water detectors. With a 3-meter-high WCD and an energy loss of 2 MeV/cm, muons can deposit a maximum of 600 MeV, as indicated in Figure 7. At this altitude, the WCD detects more energy from muons generated by protons than by iron nuclei at primary energies below 1.12 TeV. This suggests that below this energy threshold, sensitivity to iron showers decreases significantly. This consideration is crucial when calculating the cosmic ray energy spectrum in this low-energy range.

Discussions and Conclusions

This study has successfully parameterized the muon deposition at detection levels, which varies with the mass and energy of primary cosmic ray particles, using data from simulations conducted with the CORSIKA 7.7410 program. The simulations revealed that the critical energy Eα, above which heavier nuclei start to deposit more muons than protons, decreases significantly with altitude. At sea level, Eα is approximately 2.11 TeV, but it drops to less than 0.45 TeV at 10,000 meters above sea level (masl). This decrease is primarily due to the higher probability of low-energy muons, generated by showers initiated by heavier nuclei, decaying before reaching the ground.

At primary energies below $E\alpha$, protons produce more muons than iron nuclei; however, at higher energies, iron nuclei generate more muons. The simulations show that iron-initiated showers reach their maximum muon production at shallower atmospheric depths compared to proton showers. These muons, however, tend to decay more rapidly due to their lower initial energies, resulting in fewer muons being detected at greater depths. Although iron showers produce a larger number of muons, these muons generally have lower energies than those produced by proton-initiated showers. In low-energy iron showers, many muons with energies below 2 GeV decay before they can be detected. At sea level, the average energy of muons from iron nuclei is higher than at 4800 and 10,000 masl due to the more rapid decay of low-energy muons at higher altitudes.

For observatories located at 4800 masl, proton showers with energies below 1.12 TeV produce a stronger signal in Cherenkov Water Detectors (WCD) compared to those initiated by iron nuclei with the same energy. At all observation levels, muons from proton showers, on average, exhibit higher energies than those from iron-initiated showers.

These findings are particularly relevant for the measurement of low-energy cosmic ray mass composition and individual particle energy spectra. As cosmic ray observatories like LHAASO and SWGO focus on studying the cosmic ray spectrum across a wide range of energies, understanding the altitude dependent behavior of muonic components in air showers is crucial. The ability to distinguish between different primary particles based on their muonic signatures enhances the precision of cosmic ray composition studies. This research contributes to refining the reconstruction of the energy spectra and elemental composition of low-energy cosmic rays, a key area of interest in understanding cosmic ray origins and propagation in the galaxy.

This study has limitations that may impact the generalizability of its findings. First, it only simulated vertical showers, limiting applicability to non-inclined events, while real-world showers vary in angle and muon trajectory. Expanding simulations to include inclined showers would improve understanding across observation angles. Additionally, the study considered only five altitudes, missing some potentially significant intermediate levels; exploring more altitudes could clarify altitude-dependent variations in critical energy E_α and muon deposition. Lastly, with only 1000 simulated showers, statistical fluctuations might affect precision; increasing this count in future work would enhance result reliability, especially at low energies.

In summary, while this study lays a solid foundation for investigating altitude-dependent muon production and energy spectra, addressing these limitations in future research—such as incorporating a broader range of angles, additional altitudes, and larger sample sizes—will enhance the accuracy and applicability of the findings for cosmic ray observatories at diverse altitudes and orientations.

Acknowledgements
We extend our sincere gratitude to the National University of San Agustin for its invaluable support in making this research possible, thanks to the funding provided by UNSA under contract No. IBAIB-35-2020-UNSA.

Furthermore, we would like to express our appreciation to our colleagues for their insightful discussions and constructive feedback throughout the duration of this research project.

References

1. Di Sciascio G (2022) Measurement of Energy Spectrum and Elemental Composition of PeV Cosmic Rays: Open Problems and Prospects. Appl Sci 12: 705.
2. Gaisser TK, Engel R, Resconi E (2016) Cosmic Rays. In Cosmic Rays and Particle Physics, 2nd ed.; Cambridge University Press: Cambridge: 1-3.
3. Piazzoli BD, Liu SM, della Volpe D, Cao Z, Chiavassa A, et al. (2022) Chapter 4 Cosmic-Ray Physics Chin Phys C 46: 030004.
4. Boezio M, Munini R, Picozza P (2020) Cosmic Ray Detection in Space. Progress in Particle and Nuclear Physics 112: 4-5.
5. Albert A, Alfaro R, Alvarez C, Angeles Camacho JR, Arteaga-Velazquez JC, et al. (2022) Cosmic Ray Spectrum of Protons Plus Helium Nuclei Between 6 and 158 TeV from HAWC Data. Phys Rev D 105: 063021.
6. Schoorlemmer H, Hinton J, Lopez-Coto R (2019) Characteristics of Extensive Air Showers Around the Energy Threshold for Ground-Particle-Based γ-Ray Observatories. Eur Phys J C 79: 427.
7. Alfaro R, Alvarez C, Alvarez JD, Arceo R, Arteaga-Velazquez JC, et al. (2017) All-Particle Cosmic Ray Energy Spectrum Measured by the HAWC Experiment from 10 to 500 TeV. Phys Rev D 96: 122001.
8. Cao Z, Aharonian F, Axikegu, Bai YX, Bao YW, et al. (2024) Measurements of All-Particle Energy Spectrum and Mean Logarithmic Mass of Cosmic Rays from 0.3 to 30 PeV with LHAASO-KM2A. Phys Rev Lett 132: 131002.
9. Tian X, Li Z, Gou Q, Zhang H, He H, et al. (2024) Approach for Composition Measurement of Cosmic Rays Using the Muon-toElectron Ratio Observed by LHAASO-KM2A. Phys Rev D 110: 043030.
10. Zhang H, He H, Feng C (2022) Approaches to Composition Independent Energy Reconstruction of Cosmic Rays Based on the LHAASO-KM2A Detector. Phys Rev D 106: 123028.
11. Abreu P, Albert A, Alfaro R, Alvarez C, Arceo R, et al. (2019) The Southern Wide-Field Gamma-Ray Observatory (SWGO): A Next-Generation Ground-Based Survey Instrument for VHE Gamma-Ray Astronomy. arXiv: 1-20.
12. Bass SA, Belkacem M, Bleicher M, Brandstetter M, Bravina L, et al. (1998) Microscopic Models for Ultrarelativistic Heavy Ion Collisions. Prog Part Nucl Phys 41: 255-369.
13. Ostapchenko S (2006) QGSJET-II: Results for Extensive Air Showers. Nucl Phys B Proc Suppl 151: 147-150.
14. Fedynitch A, Becker Tjus J, Desiati P (2012) Influence of Hadronic Interaction Models and the Cosmic Ray Spectrum on the High Energy Atmospheric Muon and Neutrino Flux. Phys Rev D 86: 114024.
15. Knapp J, Heck D, Sciutto SJ, Dova MT, Risse M (2003) Extensive Air Shower Simulations at the Highest Energies. Astropart Phys 19: 77-99.
16. Heck D, Knapp J, Capdevielle JN, Schatz G, Thouw T, et al. (1998) CORSIKA: A Monte Carlo Code to Simulate Extensive Air Showers. Report FZKA 6019: 11.
17. National Centers for Environmental Information. Magnetic Field Calculators. NOAA National Centers for Environmental Information. https://www.ngdc.noaa.gov/geomag/calculators/magcalc.shtml?useFullSite=true
18. Cazon L, Conceicao R Riehn F (2023) Universality of the Muon Component of Extensive Air Showers. J Cosmol Astropart Phys 03: 022.
19. Cazon L, Conceicao R, Pimenta M, Santos E (2012) A Model for the Transport of Muons in Extensive Air Showers. Astropart Phys 36: 211-223.
20. Matthews J (2005) A Heitler Model of Extensive Air Showers. Astropart Phys 22: 387-397.
21. Engel J, Gaisser TK, Lipari P, Stanev T (1992) Nucleus-Nucleus Collisions and Interpretation of Cosmic-Ray Cascades. Phys Rev D 46: 5013-5025.